Study on clogging mechanism of fibrous materials in a pump by experimental and computational approaches

H Kudo[1], T Kawahara[1], H Kanai[1], K Miyagawa[1], S Saito[1] M Isono[2], M Nohmi[2], H Uchida[2], M Kawai[2]

[1]Waseda University Faculty of Science and Engineering

[2]EBARA CORPORATION

E-mail:lafayette@fuji.waseda.jp

Abstract. Clogging trouble in a sewage pump is a serious problem caused by foreign substances like strings, towels, and cloths. However, mechanism of pump clogging is significantly complicated and it is difficult to clarify factors affecting pump clogging. In this paper, the simplified air duct test and axial fan test are introduced and some parameter studies based on design of experiments (DOE) were conducted. From the DOE results, the sensitivity of each parameter to the clogging was predicted. As the parameters related to the clogging, length and rigidity of the strings, leading shape and lean angle of obstacles, flow velocity in a measuring section were selected. Behavior of string in the pump was also observed in the actual pump apparatus and was compared to that in the air duct. Computational simulation with simplified flow fields and MBD (Multi Body Dynamics) was developed and applied to predict behavior of a string in the pump. These experiments and computation are effective to detect and classify the clogging mechanism. These approaches aided to establish one of the evaluation methods on anti-clogging performance against fibrous materials.

1. Introduction

Sewage systems collect wastewater containing various foreign substances discharged from households and parks. They use a multitude of pumps for sewage transfer, which may fail due to clogging by such substances, resulting in lavatory failure or other serious problems. To prevent these problems, sewage pumps are required to resist clogging by foreign substances, i.e., to be anti-clogging, in addition to enhanced efficiency. Sewage pumps have been extensively studied regarding internal flow and performance estimation to maximize both anti-clogging performance and pump efficiency[1][2][3][4]; the results of these studies have been incorporated in the design of flow passage geometries. As low head hydropower turbine technology is drawing attention in connection with the effective use of renewable energy, studies on different aspects of clogging by foreign substances in river water are also underway.

The anti-clogging performance of sewage pumps is often represented by the “impeller passage diameter”, which shows the size of spherical solids able to physically pass through the pump impeller. A wide variety of pump types with large impeller passage diameters are available; typical sewage pump types are shown in figure 1.

In most cases, however, pump clogging is caused by accumulation of fibrous material, including towels, clothes, and paper diapers, not solids. Therefore, string was selected as a typical example of fibrous material[5][6].

This study has examined clogging mechanism and evaluated anti-clogging performance of pumps against string with element tests and actual vortex pump.

Type	Configuration	Features
Non clog	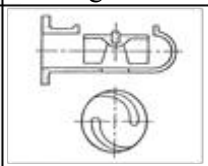	Securing a passage area between vanes by reducing the number of vanes
One vane	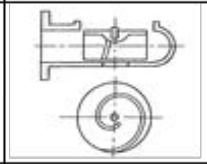	Securing a passage area by using a single spiral vane
Vortex	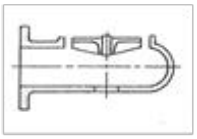	Securing a large passage area by providing a large space between the front side vanes and the casing

Fig.1 Sewage pump types

2. Element tests related to anti-clogging performance

2.1. Examination of factors affecting turbomachinery clogging based on axial fan test

To reveal clogging mechanism of pump, test using axial fan was conducted, which confirmed that string could pass through the axial fan or not. Figure 2 shows the schematic and actual test apparatus of axial fan. The specifications of the axial fan under test are as follows, a rating rotational speed of 870 min^{-1} , a rating discharge of 13.5m^3/min, an outer diameter of impeller of 250mm, an inner diameter of impeller of 94mm, a axial direction length of impeller of 31mm, a number of blades of 5, and a swept-forward skew blade. Rotational speed of the fan and the length of string were set as parameters. Rotational speed of the fan could be varied by the slidac.

To catch state of string wrapping around the blade, the high-speed video camera (element resolution 640×480, 4000fps) was used for visualization.

In this test, coefficients as follows were used. Probability of passing was defined as following formula. 50 strings in total were introduced into the fan one by one and the number of string passed through the pump was counted.

P : Probability of passing =Np/N×100 %
N : Number of string introduced into the fan
Np : Number of string passed through the fan

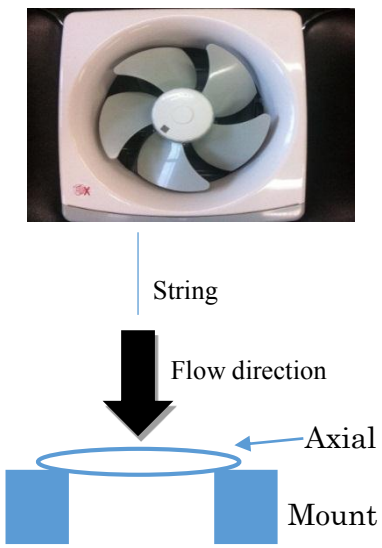

Fig.2 Schematic test apparatus of axial fan test

(1) Transit time of string

l_a : Length of vane in axial direction m

l_r : Length of string m

t_r : Transit time $= (l_r + l_a)/v_r$ s

v_r: Velocity of string m/s

(2) Transit time of one pitch of impeller

t_i : Transit time of one pitch of impeller $= 60/(nz_i)$ s

n : Rotational speed min^{-1}

z_i:Number of blades

(3) Speed coefficient

k_i : A ratio of transit time to transit time of one pitch of impeller

$= t_r / t_i = ((l_r + l_a)/v_r)(nz_i/60) = n(l_r + l_a)z_i/60v_r$

(4) An angle of flow

α : An angle of flow $= \tan^{-1}(v_f/u_i)$

u_i : Rotational speed of impeller $= \pi Dn/60$ m/s

v_f: Speed in meridian plane m/s

w : Relative speed $= \sqrt{v_f^{\,2} + u_i^{\,2}}$ m/s

Table 1 shows the combination of the flow rate (rotational speed) and the length of string, which is the condition in the test. The flow rate and the length of string were varied according to table 1. The probability of passing of each condition was shown in figure 3. This figure reveals that the probability of passing increases as discharge increases, conversely, probability of passing decreases as length of string increases. Figure 4 shows the relation between the speed coefficient described above and the probability of passing.

As shown in figure 5, the string introduced into axial fan was entangled on the blade after the string collided with the leading edge of the blade in most cases. That may be happened if friction force between a string and a blade exceeds fluid force acting on a string.

Table 1 Probability of passing P of each test condition

		String length l_r mm			Probability of passing P
		100	150	200	Average
Flow velocity v_f m/s (Rotational speed min^{-1})	1.23 (350)	**P=**0.8 (k_i =3.11)	**P=**0.55 (k_i =4.29)	**P=**0.2 (k_i =5.48)	0.52
	2.45 (700)	**P=**0.94 (k_i =3.12)	**P=**0.6 (k_i =4.31)	**P=**0.36 (k_i =5.5)	0.63
	3.68 (1050)	**P=**0.9 (k_i =3.11)	**P=**0.85 (k_i =4.30)	**P=**0.6 (k_i =5.49)	0.78
Probability of passing P	Average	0.88	0.67	0.39	

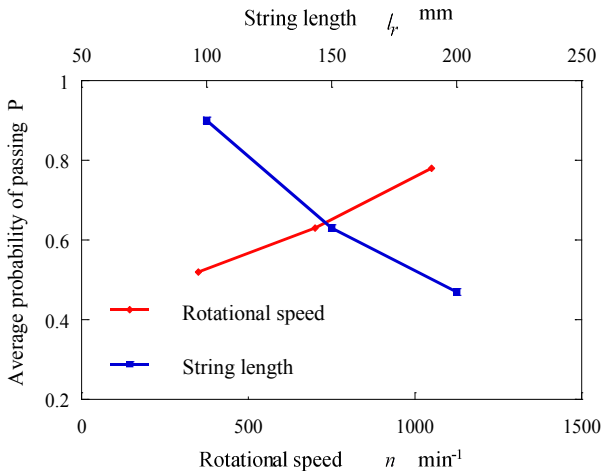

Fig.3 Response graph of the axial fan

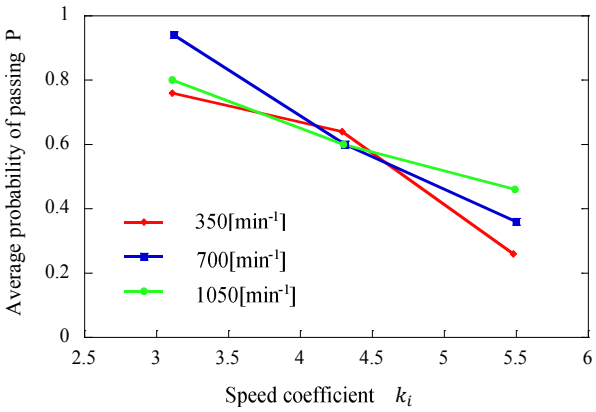

Fig.4 Passing probability by speed coefficient

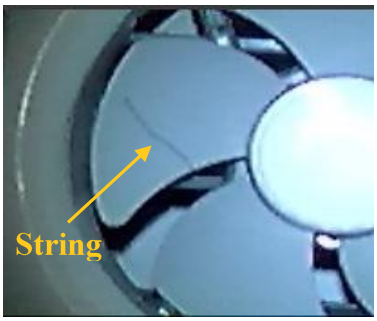

Fig.5 String entangling on the edge of the axial fan

2.2. Examination of clogging mechanism based on air duct tests

For further analysis of clogging mechanisms in the axial fan, the anti-clogging performance test based on the air duct was conducted. To simplify phenomena in rotating frame, the air duct and some obstacles were used in the static frame. Columns and triangular prisms were set in the air duct as obstacles, which represented blades in rotating frame. This test was carried out based on design of experiment to examine control factors affecting clogging[7][8].

Figure 6 shows the test apparatus which consists of circle and rectangular ducts and the blower set in bottom of the duct. As was the test of 2.1., strings were introduced into duct one by one from the top of the duct. The blower under test has a rating flow rate of 16m^3/min and a rating rotating speed of 3000min^{-1}. The length of air duct is 2.6 m and the test section where obstacles were set in has a rectangular cross section of 86mm×74mm. Since the relation between the flow velocity and the rotational speed is linear, the flow velocity was controlled by the inverter and the flow velocity at the rectangular duct section was set at 24 m/s through the whole test. Figure 7 shows the columns and the triangular prisms under test which have lean angle of 0°,10°,20°.

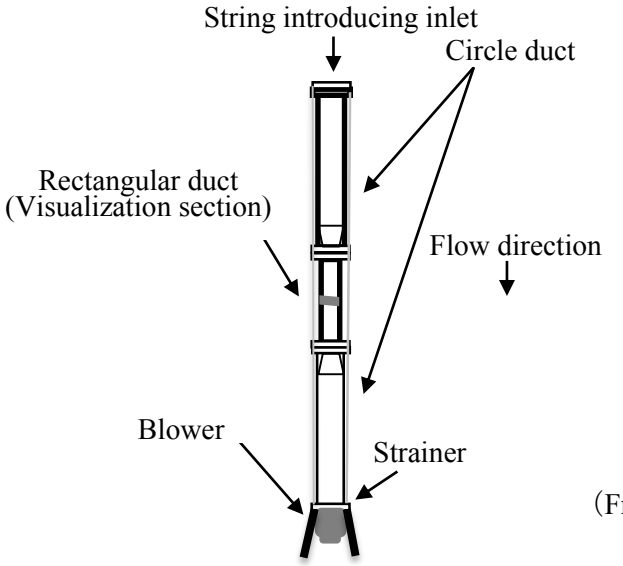

Fig.6 Schematic test apparatus of air duct test

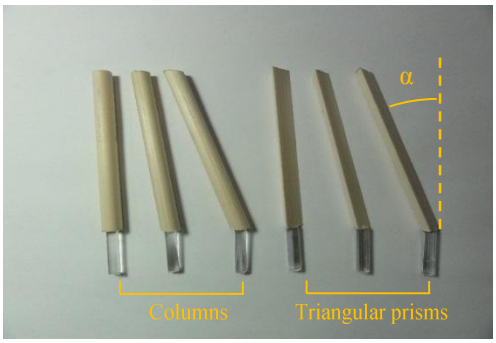

Fig.7 Columns and triangular prisms under test
(From the left, a lean angle α of 0°,10°,20°respectively)

Figure 8 shows the velocity triangle at inlet of axial fan and the arrangements of the columns and the triangular prisms in the air duct. As shown in figure 8, 5 columns and triangular prisms each were set with slope arrangement to represent the relation between a string and blades in relative frame of axial fan.

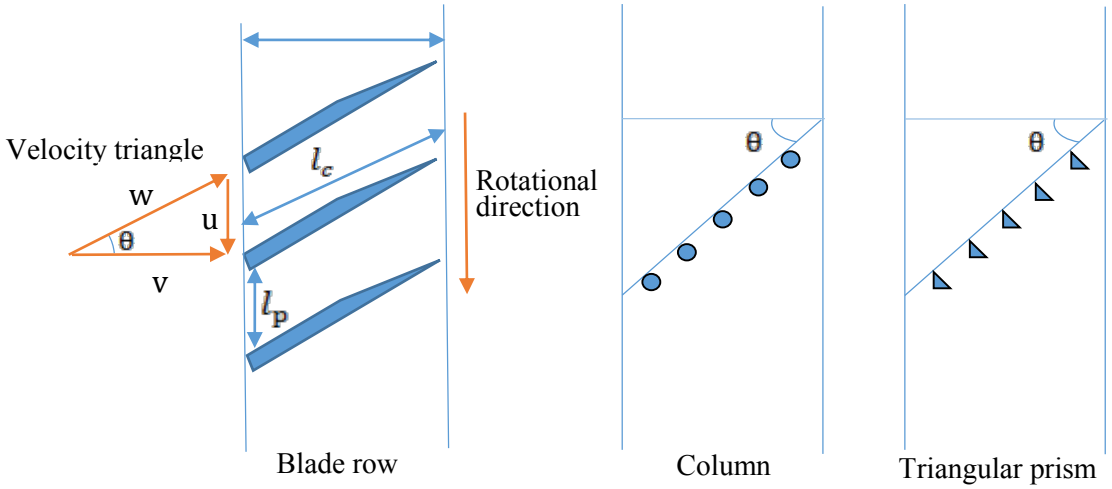

Fig.8 Arrangement of obstacles

Table 2 shows the combination of the control factors and levels. The shape of the obstacle, lean angle, string material, surface roughness, string length, and flow velocity are selected as the control factors, then each control factor has two or three levels. Figure 9 shows the response graph based on the results of air duct test. This figure indicates that the probability of passing varies according to length and material of string, surface roughness and shape of obstacles. Figure 10 shows the string entangling on the obstacle.

Table 2 Combination of the control factors and levels

		Levels		
		1	2	3
Control factors	Shape	○	△	—
	Lean angle °	0	10	20
	String materials	Polyester	Cotton	Rubber
	Surface roughness of obstacles	#600	#2000	#5000
	String length mm	150	250	350
	Flow velocity m/s	15	20	25

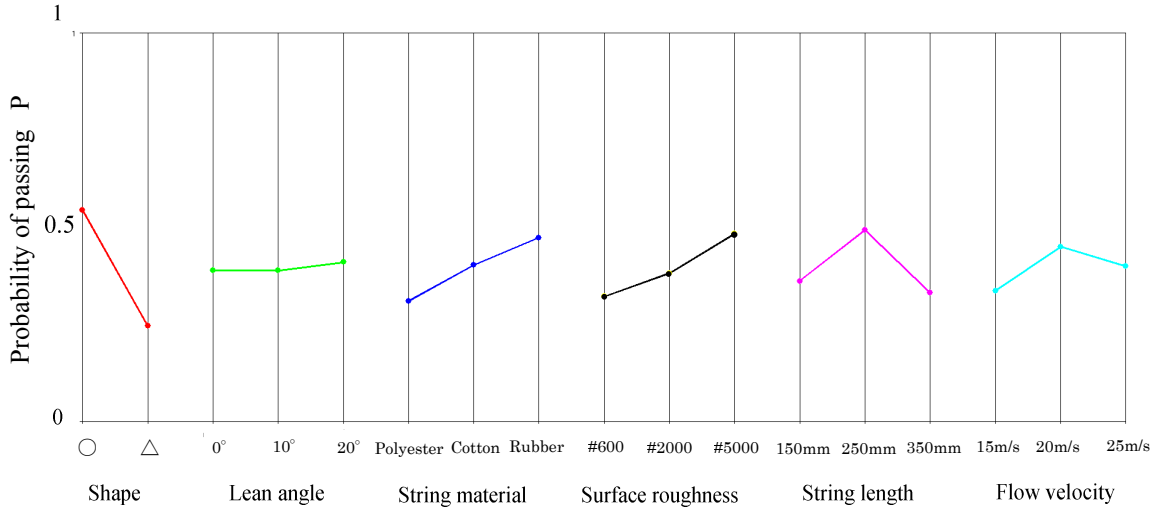

Figure 9. Response graph of the air duct test

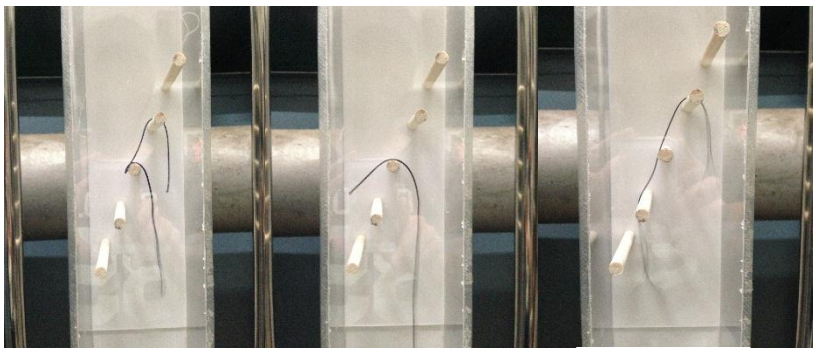

(a) Polyester (b) Cotton (c) Rubber

Fig.10 String entangling on the columns

2.3. Comparison between axial fan and air duct test

The results of both axial fan and air duct tests are shown in figure 11, in the forms of the relation of the probability of passing and the length of string, provided that the length of string was made dimensionless by the pitch between obstacles. This graph reveals that curves of both tests are different, however the probability of passing and the slope of them are almost same within a range of small ratio of string length to pitch. These facts suggest that if the ratio of string length to pitch is in the range of

1~1.5, it can be possible to represent clogging in the rotating frame with air duct test apparatus in static frame.

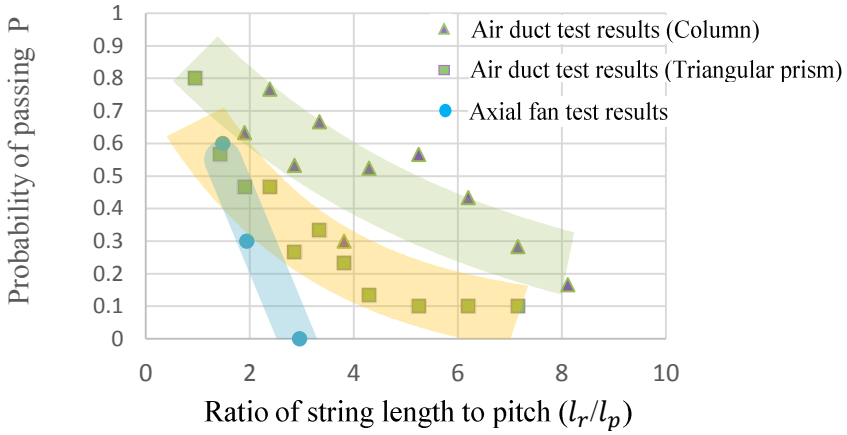

Fig.11 Relation between the probability of passing (P) and the ratio of string length to pitch (l_r/l_p)

3. Computational simulation of fibrous material and fluid

In this chapter, for an aim to simulate the fibrous materials like a string in the rotating fluid field of pump, computational simulation of the simplified flow field and the fibrous material was calculated to examine validity of analysis methodology.

3.1. Analysis methodology

To represent flexible fibrous material like string, ANCF (Absolute Nodal Coordinate Formulation) [9] was used and string motion in flow field was simulated with one-way coupling.

3.2. Formulation of ANCF

ANCF is the one kind of non-linear finite element methods, which represents large rigid body motion and deformation rigidly. The flexible string is divided into some rigid bodies and bodies are connected with nodes each other. Since nodes between rigid bodies are defined in an absolute coordinates, displacement and rotation of a rigid body can be represented accurately.

- Formulation of equation of motion

Assume that a rigid body is Euler-Bernoulli beam, the equation of motion is expressed as follow with mass matrix $\boldsymbol{M}$, generalized coordinate $\boldsymbol{q}$, external force $\boldsymbol{Q_f}$ and elastic force $\boldsymbol{Q_k}$.

$$\boldsymbol{M\ddot{q}} = \boldsymbol{Q_f} - \boldsymbol{Q_k} \tag{1}$$

Furthermore, elastic force is expressed as a combination of elastic force against extension displacement $\boldsymbol{Q_l}$ and bending deflection $\boldsymbol{Q_t}$.

$$\boldsymbol{Q_k} = \boldsymbol{Q_l} + \boldsymbol{Q_t} \tag{2}$$

While mass matrix $\boldsymbol{M}$ and elastic force against bending deflection $\boldsymbol{Q_t}$ are constant values, external force $\boldsymbol{Q_f}$ and elastic force against extension displacement $\boldsymbol{Q_l}$ are time variable. Thus, it is necessary to calculate $\boldsymbol{Q_l}$ at every time step of numerical integration.

- Formulation of external force

$$\boldsymbol{F_1} = \frac{1}{2}\rho C_D A|\boldsymbol{U}|\boldsymbol{U} \tag{3}$$

Where drag force applied to a rigid body in unsteady flow is $\boldsymbol{F}_1$, form drag coefficient is C_D, projected area is A, and relative speed between rigid body and flow is $\boldsymbol{U}$.

Although added mass effect is normally taken count in unsteady flow, form drag assume to be large enough compare to added mass effect in this simulation. Therefore, external force $\boldsymbol{Q_f}$ is expressed as follow.

$$\boldsymbol{Q_f} = \boldsymbol{F_1} = \frac{1}{2}\rho C_D A|\boldsymbol{U}|\boldsymbol{U} \tag{4}$$

3.3 Simulation of string behavior

The behavior of the flexible string formulated in 3.2 in simplified flow field was simulated. Condition under simulation is shown below.

Figure 12, 13 shows the simplified flow field for the simulation. Positive random flow was given in figure 12 and band-shaped flow in opposite direction was given in figure 13. The string simulated consisted of 10 rigid bodies and each body has a length of l and square cross section with side length of d. Aspect ratio A of rigid body was defined $A = l/d$. Actual distances along x-axis and y-axis were made dimensionless by d and expressed X, Y respectively.

Analysis Condition

A : Aspect ratio =10
d×d : Cross section area of rigid body =$(1 \times 10^{-3}) \times (1 \times 10^{-3})$ m^2
E : Elastic modulus =1×10^4 N/m^2
I : Moment of inertia of area = 1×10^{-9} m^4
l : Length of rigid body =1×10^{-2} m
l_r : Length of string =1×10^{-1} m
N : Number of rigid bodies =10
T : Analysis time =10 s
Δt : Time step = 0.01 s
ρ : Density of rigid body =7850 kg/m^3
Method for numerical integration：Runge-Kutta 4th order method

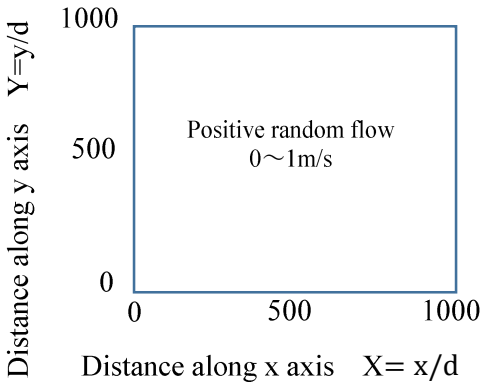

Fig.12 Flow field (Random flow)

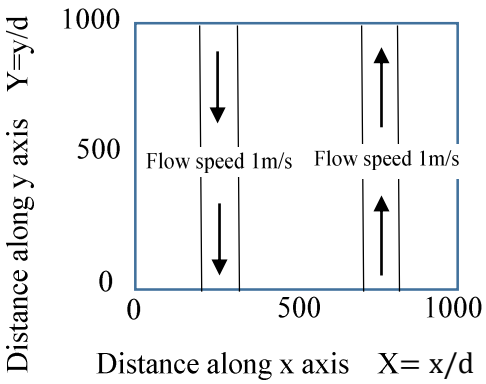

Fig.13 Flow field (Band-shaped flow)

3.4 Simulation results

The results of string behavior at every 2 seconds is shown in figure 14, 15. Initial nodal position (X,Y) was (450~550,500), and the velocity of all nodes was 0.

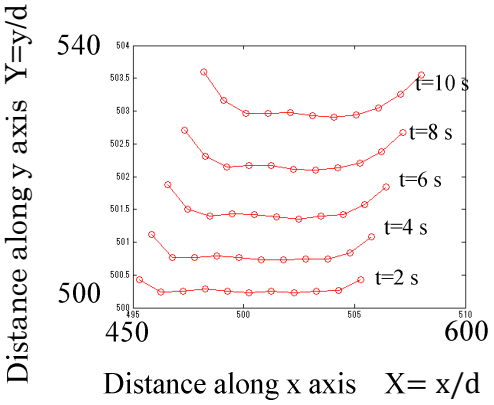

Fig.14 String behavior (Random flow)

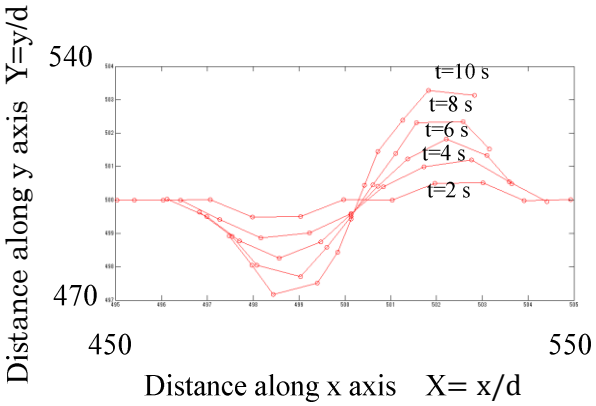

Fig.15 String behavior (Band-shaped flow)

4. Clogging of vortex pump

4. 1 Clogging test of vortex pump

Closed loop test apparatus which has tank and visualization section of vortex pump was used in this test. With this apparatus, it is possible to visualize influx of string and clogging in a pump by using a high-speed video camera.

The purpose of this test is to observe behavior of string in the actual pump. Anti-clogging performances at design point of pump and other operating points with varying the length of string were examined. The strings under test had three kinds of length, which were 1D, 2D and 4D, where D is pipe diameter of pump inlet.

4. 2 Internal flow analysis of vortex pump

The internal flow of vortex pump shown in figure 16 was analyzed using CFD method. The analysis condition is shown in table 3.

Figure 17~19 shows oil flow at the impeller, total pressure, and loss contour at meridian plane respectively. These results indicates that flow in the vortex pump is significantly complicated.

There are three flow patterns observed in the results. One is the flow passes through the vanes smoothly. Second is the vortex flow dragged by rotational motion of impeller. Third is the vortex flow between pump casing and impeller, which is observed at meridian plane.

Table 3 Analysis condition

Model		
Element number	6256297	-
Node number	1842996	-
Conditions		
Turbulence model	RANS standard k-ε model	
Time step	0.0005	s
Working fluid	Water（incompressible20℃）	
Boundary condition of inlet (Flow rate)	0.2244	m^3/min
Boundary condition of outlet (Total pressure)	0	Pa
Rotational speed	2000	min^{-1}

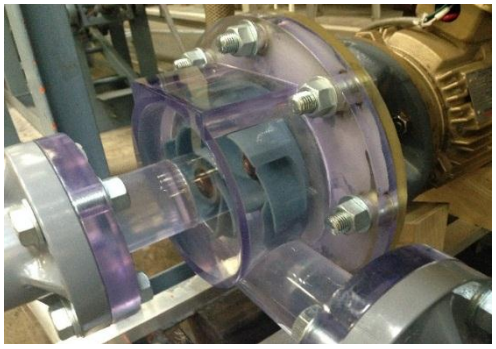

Fig.16 Visualization section of vortex pump

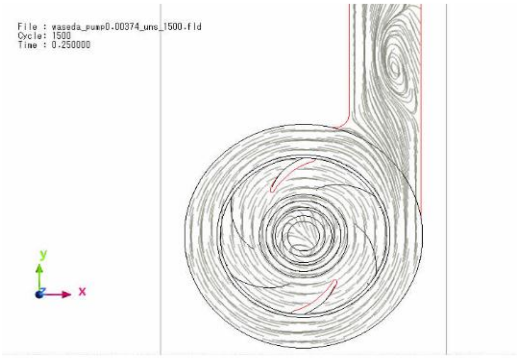

Fig.17 Streamline at the impeller

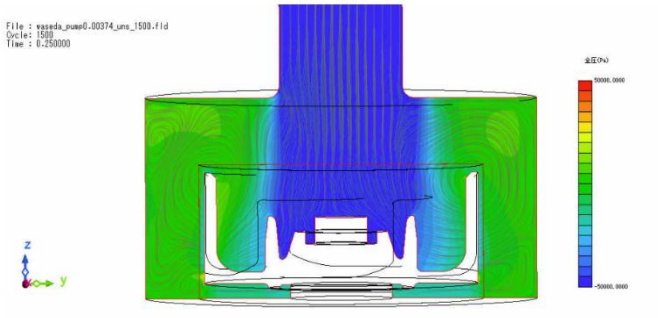

Fig.18 Total pressure contour

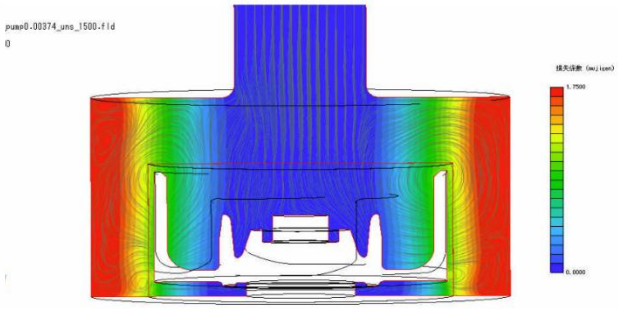

Fig.19 Loss contour

4.3 Test results of clogging of vortex pump

Strings with a variety of length were introduced into vortex pump one by one, then string behavior in the pump casing was observed using the high-speed video camera. This test was conducted under the constant flow rate of 0.2033 m^3/min. Figure 20 shows the state of strings entangling on the leading edge of the vane.

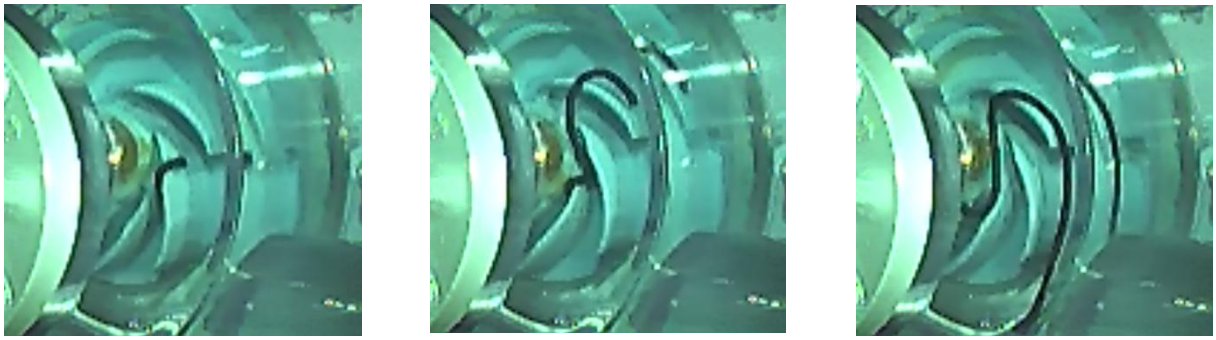

(a) l_r=1D (b) l_r=2D (c) l_r=4D

Fig.20 String entangling on the blade
(D : Pipe diameter of the pump inlet = 50mm)

This visualization reveals four following findings.

- The trend was observed that strings go with the vortex flow in the pump casing with relatively stretched position along with the shape of the vane.
- Strings can be entangled on the leading edge of the vane for a few moment even if the vane is skewed
- Longer strings were more likely to entangle on the leading edge of two or more vanes.
- It was observed that strings passed through vanes and come back to the impeller boss area.

5. Conclusion

The conclusions obtained from all the tests to examine clogging mechanism and evaluate the anti-clogging performance of the vortex pump are as follows.
(1) From the response graphs of the axial fan and air duct tests, string length, surface roughness of obstacles, string material, and shape of leading edge significantly affect the probability of passing.
(2) The results of probability of passing obtained from axial fan test suggest that the speed coefficient is suitable to evaluate the anti-clogging performance.
(3) To compare air duct test and axial fan test, a ratio of string length to pitch was introduced instead of speed coefficient. Therefore, it can be possible to represent the entangling and clogging in rotating frame with the air duct test apparatus in static frame, if the ratio of string length to pitch is in the range of 1~1.5.
(4) The complicated vortex flow field was simulated in the CFD, which was also observed in the visualization of string behavior in vortex pump.
(5) It was confirmed that the string behavior and characteristics of clogging in vortex pump were similar to that in the air duct test. This fact leads to the possibility that phenomena in rotational frame could be imitated in static frame.
(6) Absolute nodal coordinate formulation allows us to simulate flexible string in the flow field.

References

[1] Aoki, Studies on the Vortex Pump : First Report, Internal Flow, Transactions of the Japan Society of Mechanical Engineers B, 48-431, 1982-7,1292 (in Japanese)A reference
[2] Aoki, Studies on the Vortex Pump : Second Report, Pump Performance, Transactions of the Japan Society of Mechanical Engineers B, 48-431, 1982-7,1300 (in Japanese)
[3] Aoki, Studies on the Vortex Pump : Third Report, Predicting Cavitation Characteristics, Transactions of the Japan Society of Mechanical Engineers B, 48-434, 1982-10,1963 (in Japanese)
[4] Aoki, Studies on the Vortex Pump : Fourth Report, Internal Flow, Transactions of the Japan Society of Mechanical Engineers B, 48-434, 1982-10,1969 (in Japanese)
[5] Isono, Nohmi, Uchida, Kawai, Kudo, Kawahara, Miyagawa, Varification of the mechanism of pump clogging and anti-clogging performance evaluation method, Proceedings of the Turbo machinery Society of Japan Conference, 2013-9, EBARA CORPORATION, Waseda University (in Japanese)
[6] Isono, Nohmi, Uchida, Kawai, Kudo, Kawahara, Kanai, Miyagawa, Saito, An experimental study on pump clogging, International Association for Hydro-Environment Engineering and Research (upcoming), 2014-9, EBARA CORPORATION, Waseda University.
[7] Morita, Fundamental and Arrangement of Experimental Design, Shuwa System, 2013-2, p.10-232
[8] Tatebayashi, Introduction to Taguchi method, Kagiren publishing, 2009-10, p.1-74,p.221-247
[9] Multibody Dynamics (2) –Numerical Analysis and Applications-, The Japan Society of Mechanical Engineers, 2007-9, p.108-238